

Article

# Universal Dependence of Nuclear Spin Relaxation on the Concentration of Paramagnetic Centers in Nano- and Microdiamonds

Alexander M. Panich

Department of Physics, Ben-Gurion University of the Negev, Beer-Sheva 8410501, Israel; pan@bgu.ac.il

**Abstract:** An analysis of our data on  $^1\text{H}$  and  $^{13}\text{C}$  spin–lattice and spin–spin relaxation times and rates in aqueous suspensions of purified nanodiamonds produced by detonation technique (DNDs), DNDs with grafted paramagnetic ions, and micro- and nanodiamonds produced by milling bulk high-temperature high-pressure diamonds is presented. It has been established that in all the studied materials, the relaxation rates depend linearly on the concentration of diamond particles in suspensions, the concentration of grafted paramagnetic ions, and surface paramagnetic defects produced by milling, while the relaxation times exhibit a hyperbolic dependence on the concentration of paramagnetic centers. This is a universal law that is valid for suspensions, gels, and solids. The results obtained will expand the understanding of the properties of nano- and microdiamonds and will be useful for their application in quantum computing, spintronics, nanophotonics, and biomedicine.

**Keywords:** spin–lattice relaxation time; spin–spin relaxation time; nanodiamonds; paramagnetic defects; concentration dependence

**Citation:** Panich, A.M. Universal Dependence of Nuclear Spin Relaxation on the Concentration of Paramagnetic Centers in Nano- and Microdiamonds. *Materials* **2022**, *15*, 5774. <https://doi.org/10.3390/ma15165774>

Academic Editor: Christian Müller

Received: 2 August 2022

Accepted: 19 August 2022

Published: 21 August 2022

**Publisher's Note:** MDPI stays neutral with regard to jurisdictional claims in published maps and institutional affiliations.



**Copyright:** © 2022 by the author. Licensee MDPI, Basel, Switzerland. This article is an open access article distributed under the terms and conditions of the Creative Commons Attribution (CC BY) license (<https://creativecommons.org/licenses/by/4.0/>).

## 1. Introduction

Detonation nanodiamond (DND) particles are of significant scientific interest and are very promising materials for modern science and applications in quantum computing, spintronics, nanophotonics, and biomedical applications due to the small size of primary particles (5 nm) with a narrow size distribution, easy surface functionalization, high biocompatibility, and possibility of production in large quantities [1–11]. DND suspensions with grafted paramagnetic metal cations [12–20] exhibit a high relaxivity and are proposed as new contrast agents for magnetic resonance imaging (MRI) [16–18,20]. Recently, Sękowska et al. reported the possible use of DNDs in MRI phantoms [21] produced using distilled water, agar, and carrageenan with the addition of the DND particles suspended in dimethyl sulfoxide (DMSO). Surprisingly, the authors obtained linear dependences of the spin–lattice ( $T_1$ ) and spin–spin ( $T_2$ ) relaxation times in the phantoms as a function of the nanodiamond concentration (see Figures 3 and 5 in Ref. [21]). This result contradicts our recent experimental nuclear magnetic resonance (NMR) data on DND suspensions [16–18], as well as some fundamentals of relaxation phenomena in nuclear spin systems [22–24].

In this paper, we analyze the results of measuring proton and carbon nuclear spin–lattice and spin–spin relaxation times and rates in (i) aqueous suspensions of highly purified DNDs, (ii) aqueous suspensions of DNDs with grafted paramagnetic ions, (iii) powdered DNDs grafted with paramagnetic ions, and (iv) powdered micro- and nanodiamonds produced by milling bulk diamonds prepared by the high-temperature high-pressure (HTHP) method. We established that in all the studied materials the relaxation rates depend linearly on the concentration of nanodiamonds in suspensions, the

concentration of grafted paramagnetic ions in suspensions and in powder samples, and surface paramagnetic defects produced by milling, while the relaxation times exhibit a hyperbolic dependence on the concentration of paramagnetic centers. This is a universal law that is valid for suspensions, gels, and solids. The results obtained will expand the understanding of the behavior of nano- and microdiamonds and will be useful for their applications in quantum computing, spintronics, nanophotonics, and particularly in biomedical applications.

## 2. Materials and Methods

We report the data on aqueous suspensions of purified DNDs and DNDs with grafted  $Gd^{3+}$  ions, powder DNDs with grafted  $Cu^{2+}$  and  $Gd^{3+}$  ions, and milled HTHP nanodiamonds of the SYP series. Sample purification, EPR, and SQUID impurities monitoring and preparation of aqueous suspensions of highly purified and de-agglomerated DND particles are described elsewhere [12–18,25]. The average DND particle size is ca. 4.5–5 nm as determined by dynamic light scattering (DLS), transmission electron microscopy (TEM), and atomic force microscopy (AFM) measurements [12–18,26].

Grafting of the nanodiamond surface with copper and gadolinium ions was made by mixing aqueous suspensions of nanodiamond particles with aqueous solutions of copper acetate  $Cu(CH_3CO_2)_2$  or gadolinium nitrate hexahydrate  $Gd(NO_3)_3 \cdot 6H_2O$  [12–18]. Dissociated metal cations ( $Cu^{2+}$  or  $Gd^{3+}$ ) in this mixture undergo ion exchange with hydrogen atoms of surface carboxyl groups and subsequent chemical bonding to the nanoparticle surface [12–15]. Thereafter, we call these materials Cu-DND and Gd-DND.

Submicron diamond powders of Syndia SYP series, manufactured by L.M. Van Moppes & Sons SA, Geneva, Switzerland, and hereafter identified by the denomination SYP, were produced by milling initial CDFS HPHT microdiamond crystallites with an average particle size of 100  $\mu m$ , which resulted in several fractions with average particle sizes of 18, 30, 86, 130, 208, and 386 nm [27]. An additional laboratory purification stage was carried out to exclude ferro- and paramagnetic impurities from the commercial SYP samples.

The EPR study of all samples of purified DNDs shows the concentration of paramagnetic defects in the range of  $(4 \div 7) \times 10^{19}$  spin/g [26,28–33], while in SYP NDs the concentration varied from  $6.7 \times 10^{18}$  to  $3.3 \times 10^{19}$  spin/g depending on the particle size [27].

It is well established that the surface of DND particles is terminated by hydrogen atoms forming hydrocarbon, hydroxyl, and carboxyl groups [30,31]. They are the source of  $^1H$  nuclear spins.  $^1H$  and  $^{13}C$  NMR measurements of powder samples were carried out at room temperature ( $T = 295$  K) using a Tecmag (Houston, TX, USA) pulse solid-state NMR spectrometer and an Oxford superconducting magnet in an external magnetic field  $B_0 = 8.0$  T, corresponding to the  $^1H$  and  $^{13}C$  resonance frequencies of 340.52 and 85.62 MHz, correspondingly.  $^{13}C$  spin–lattice relaxation times  $T_1$  were measured using a saturation comb pulse sequence ( $\frac{\pi}{2}$  pulse train) [34]. Magnetization recovery in measuring

$T_1$  was fitted by a stretched exponential  $M(t) = M_{\infty} \{1 - \exp[-(\frac{t}{T_1})^{\alpha}]\}$ , which is characteristic of the spin–lattice relaxation through paramagnetic defects [12–15,19,20,26,27–31,35]. Here,  $M_{\infty}$  is the equilibrium magnetization, and the parameter  $\alpha$  varies in the range of  $0.5 < \alpha < 1$ .  $^{13}C$  spin–spin relaxation times  $T_2$  were measured using the Hahn echo method.

$^1H$  NMR measurements of nanodiamond suspensions were carried out at a temperature of 310.1 K (37 °C). The  $^1H$  spin–lattice relaxation times  $T_1$  were measured using an inversion recovery pulse sequence [34], while the spin–spin relaxation times  $T_2$  were measured using a Carr–Purcell–Meiboom–Gill (CPMG) pulse sequence [36].

### 3. Results and Discussion

#### 3.1. Suspensions of Purified DNDs and DNDs with Grafted Paramagnetic Ions

As is known, DND particles exhibit intrinsic localized paramagnetic defects: (i) P1 nitrogen paramagnetic centers distributed over the entire diamond core and (ii) unpaired electron spins of dangling bonds positioned mainly in the near-surface layer [26,28–31]. The total defect density in DND particles measured by the EPR method is around  $6 \times 10^{19}$  spin/g [26,28–31]. In DND suspensions, the relaxation of the proton nuclear spins of the solvent is accelerated, owing to the interaction of protons with unpaired electron spins of the aforementioned paramagnetic defects [16–18]. The contributions of the DND-inherent paramagnetic defects to the experimentally measured proton spin–lattice and spin–spin relaxation rates  $R_1^{\text{exp}}$  and  $R_2^{\text{exp}}$  in suspensions are described [16–18] by the second term of the equations

$$R_1^{\text{exp}} = \frac{1}{T_1^{\text{exp}}} = \frac{1}{T_1^{\text{solv}}} + \frac{1}{T_1^{\text{DND}}} = R_1^{\text{solv}} + r_1^{\text{DND}} \times C_{\text{DND}} \quad (1)$$

$$R_2^{\text{exp}} = \frac{1}{T_2^{\text{exp}}} = \frac{1}{T_2^{\text{solv}}} + \frac{1}{T_2^{\text{DND}}} = R_2^{\text{solv}} + r_2^{\text{DND}} \times C_{\text{DND}} \quad (2)$$

where  $T_1^{\text{solv}}$  and  $T_2^{\text{solv}}$  are the relaxation times due to the solvent,  $T_2^{\text{DND}}$  and  $T_1^{\text{DND}}$  are the spin–lattice and spin–spin relaxation times caused by paramagnetic defects of the nanodiamond particles,  $C_{\text{DND}}$  is the DND concentration, and  $r_1$  and  $r_2$  are the relaxivities defined as the slopes of the concentration dependences of  $\frac{1}{T_1^{\text{exp}}}$  and  $\frac{1}{T_2^{\text{exp}}}$ . Here,  $T_1^{\text{solv}}$  and  $T_2^{\text{solv}}$  are the characteristics of the particular liquid solvent used and, therefore, are constant for all measurements.

The results of our measurements of the spin–lattice and spin–spin relaxation times and rates of water protons in aqueous DND suspensions as a function of the DND concentration are shown in Figures 1 and 2. Our data show that paramagnetic defects of the DND particles (i) affect the relaxation rates of water protons in suspension and (ii) reveal a linear dependence of the relaxation rates  $R_1^{\text{DND}}$  and  $R_2^{\text{DND}}$  on the DND content. This finding is in accordance with the fundamentals of the spin relaxation theory [22–24], which demonstrates a linear dependence of the relaxation rate on the concentration of paramagnetic centers/defects. Herewith, as it follows from Equations (1) and (2) and the experimental data presented in Figures 1 and 2, both proton spin–lattice and spin–spin relaxation times demonstrate a hyperbolic dependence on the concentration  $C_{\text{DND}}$  of nanodiamonds in suspension according to Equations (3) and (4):

$$T_1 = \frac{1}{R_1^{\text{solv}} + r_1^{\text{DND}} \times C_{\text{DND}}} \quad (3)$$

$$T_2 = \frac{1}{R_2^{\text{solv}} + r_2^{\text{DND}} \times C_{\text{DND}}} \quad (4)$$

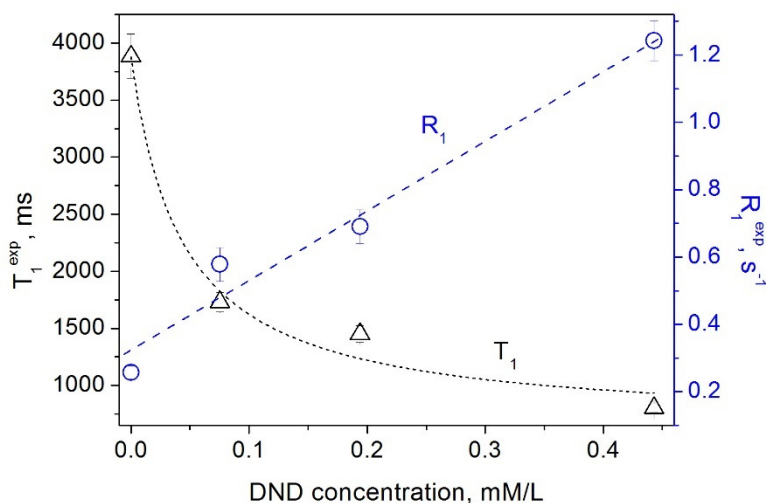


**Figure 1.** Dependence of the spin–lattice relaxation rate  $R_1$  (circles) [16] and the spin–lattice relaxation time  $T_1$  (triangles) of water protons in aqueous DND suspensions on the DND concentration.

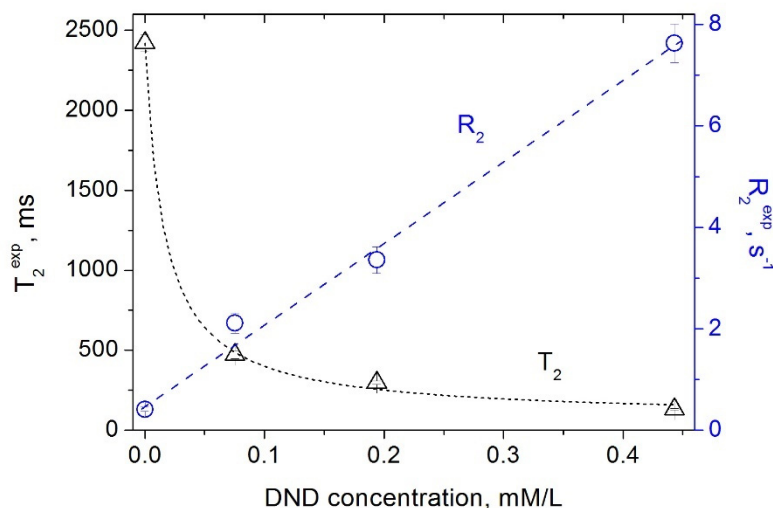


**Figure 2.** Dependence of the spin–spin relaxation rate  $R_2$  (circles) [16] and the spin–spin relaxation time  $T_2$  (triangles) of water protons in aqueous DND suspensions on the DND concentration.

This experimental result contrasts with the linear concentration dependence of  $T_1$  and  $T_2$  reported by Sękowska et al., [21]. The latter is inconsistent with that published in the literature and the fundamentals of the relaxation phenomena in nuclear spin systems, which casts some doubt on the correctness of the measurements and conclusions made in Ref. [21]. Herewith, we note that the measurements of Sekowska et al., particularly those of  $T_2$ , were carried out in a limited range of nanodiamond concentrations, which causes some difficulties in establishing the character of the concentration dependence measured by these authors.

Similar dependencies were obtained for suspensions of the gadolinium-grafted DND (Gd-DND), which are shown in Figures 3 and 4. Contributions of paramagnetic gadolinium ions grafted to the DND surface to the spin–lattice and spin–spin relaxations of water protons in this case are:

$$R_1^{\text{exp}} = \frac{1}{T_1^{\text{exp}}} = \frac{1}{T_1^{\text{Gd}}} + \frac{1}{T_1^{\text{DND}}} + \frac{1}{T_1^{\text{H}_2\text{O}}} = r_1^{\text{Gd}} \times C_{\text{Gd}} + R_1^{\text{DND}} + R_1^{\text{H}_2\text{O}} \quad (5)$$

$$R_2^{\text{exp}} = \frac{1}{T_2^{\text{exp}}} = \frac{1}{T_2^{\text{Gd}}} + \frac{1}{T_2^{\text{DND}}} + \frac{1}{T_2^{\text{H}_2\text{O}}} = r_2^{\text{Gd}} \times C_{\text{Gd}} + R_2^{\text{DND}} + R_2^{\text{H}_2\text{O}} \quad (6)$$

where  $C_{\text{Gd}}$  is the Gd(III) ions concentration in suspension.

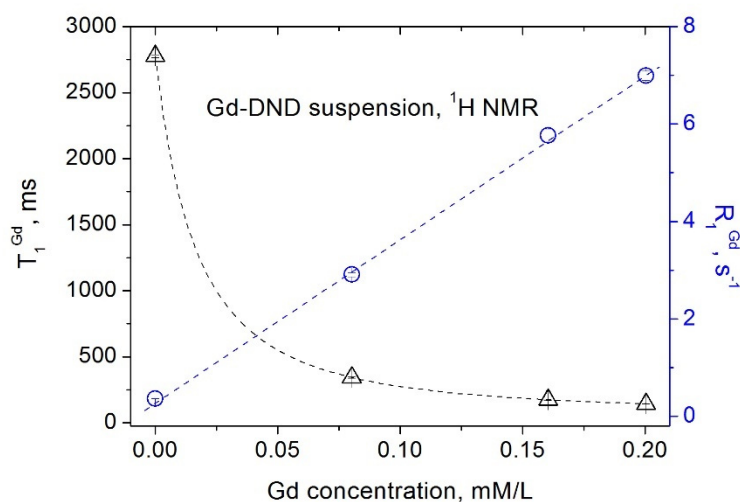


**Figure 3.** Dependence of the spin–lattice relaxation rate  $R_1$  (circles) [16] and the spin–lattice relaxation time  $T_1$  (triangles) of water protons in aqueous Gd-DND suspensions on the  $\text{Gd}^{3+}$  ion concentration.

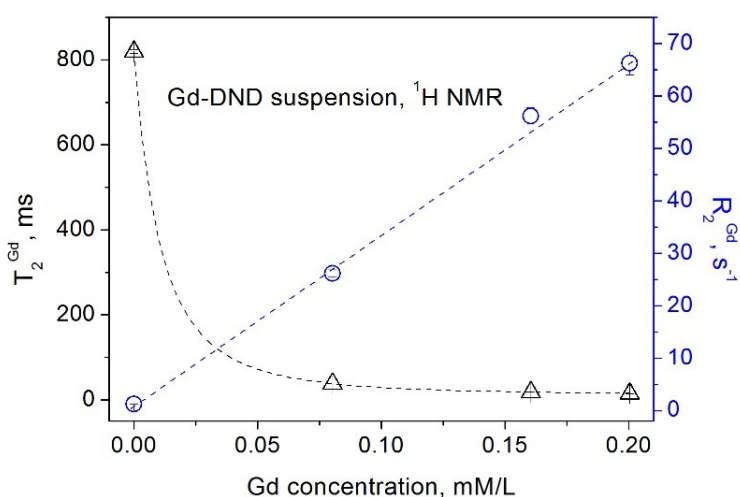


**Figure 4.** Dependence of the spin–spin relaxation rate  $R_2$  (circles) [16] and the spin–spin relaxation time  $T_2$  (triangles) of water protons in aqueous Gd-DND suspensions on the  $\text{Gd}^{3+}$  ion concentration.

Therefore, the proton spin–lattice and spin–spin relaxation times reveal a hyperbolic dependence on  $C_{\text{Gd}}$ :

$$T_1^{\text{exp}} = \frac{1}{r_1^{\text{Gd}} \times C_{\text{Gd}} + R_1^{\text{DND}} + R_1^{\text{H}_2\text{O}}} \quad (7)$$

$$T_2^{\text{exp}} = \frac{1}{r_2^{\text{Gd}} \times C_{\text{Gd}} + R_2^{\text{DND}} + R_2^{\text{H}_2\text{O}}} \quad (8)$$

We note that Gd(III) ions have a large unpaired electron spin of  $S = 7/2$  and a large magnetic moment of  $7.9 \mu_B$  (here,  $\mu_B$  is the Bohr magneton), thus their contribution to relaxation exceeds the DND contribution by more than an order of magnitude [16–18].

In addition to our data, we mention the measurements of an aqueous solution of the nanodiamond-polyglycerol-gadolinium(III) conjugate DND-PG-Gd(III) [37]. The relaxation rates  $R_1$  of water protons in this material show a linear dependence on the Gd concentration in magnetic fields of 1.5 T, 3.0 T, and 7.0 T.

### 3.2. Powder DNDs with Grafted Paramagnetic Ions

Similar dependences of the nuclear spin relaxation in nanodiamonds on the concentration of the paramagnetic ions were obtained in our measurements of powder samples. In this case, the spin–lattice relaxation rate  $R_1 = \frac{1}{T_1}$  of the nuclear spin  $I$ , which interacts with the unpaired electron spin  $S$  of the paramagnetic ion, is given by the expression [14,15,19,20,22,29–31]

$$R_1(r) = \frac{1}{T_1(r)} = \frac{2}{5} \gamma_s^2 \gamma_i^2 \hbar^2 S(S+1) \left[ \frac{3\tau_e}{1 + \omega_i^2 \tau_e^2} \right] \left( \frac{1}{r^6} \right) \times N_s \quad (9)$$

Here,  $\gamma_i$  and  $\gamma_s$  are the nuclear and electron gyromagnetic factors,  $\omega_i$  is the nuclear Larmor angular frequency,  $r$  is the distance from the nucleus to the paramagnetic ion,  $\tau_e$  is the correlation time of the electron spin of the paramagnetic ion, and  $N_s$  is the number of paramagnetic ions in the particle.

The obtained dependences of the  $^1\text{H}$  and  $^{13}\text{C}$  spin–lattice relaxation times and rates on the concentration of paramagnetic  $\text{Cu}^{2+}$  and  $\text{Gd}^{3+}$  ions grafted to the DND surface are presented in Figures 5–8. All these data show a linear dependence of the spin–lattice and spin–spin relaxation rates  $R_1$  and  $R_2$  and a hyperbolic dependence of the relaxation times  $T_1$  and  $T_2$  on the paramagnetic ions concentration. This finding is consistent with the fundamentals of the spin relaxation theory [22–24], which demonstrates a linear dependence of the relaxation rate on the concentration of paramagnetic centers.

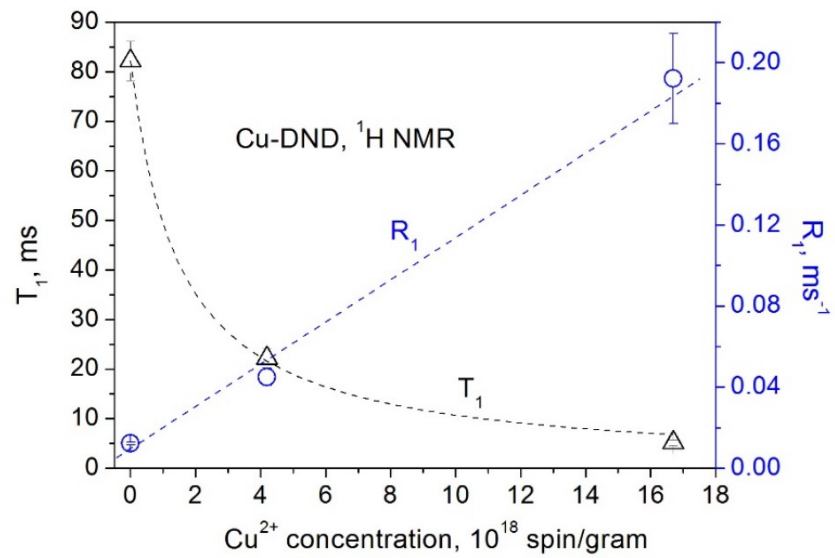


**Figure 5.** Dependence of the  $^1\text{H}$  spin–lattice relaxation rate  $R_1$  (circles) and the spin–lattice relaxation time  $T_1$  (triangles) in Cu-DND powders on the  $\text{Cu}^{2+}$  ion concentration.

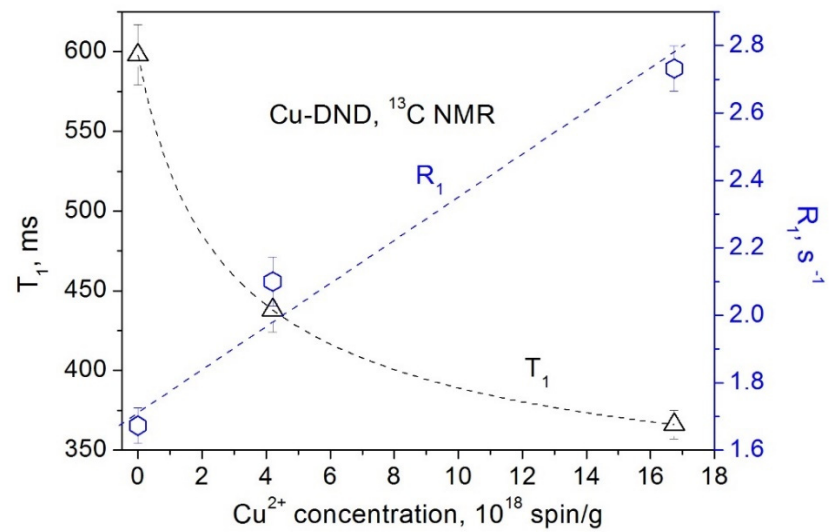


**Figure 6.** Dependence of the  $^{13}\text{C}$  spin–lattice relaxation rate  $R_1$  (circles) and the spin–lattice relaxation time  $T_1$  (triangles) in Cu-DND powders on the  $\text{Cu}^{2+}$  ion concentration.

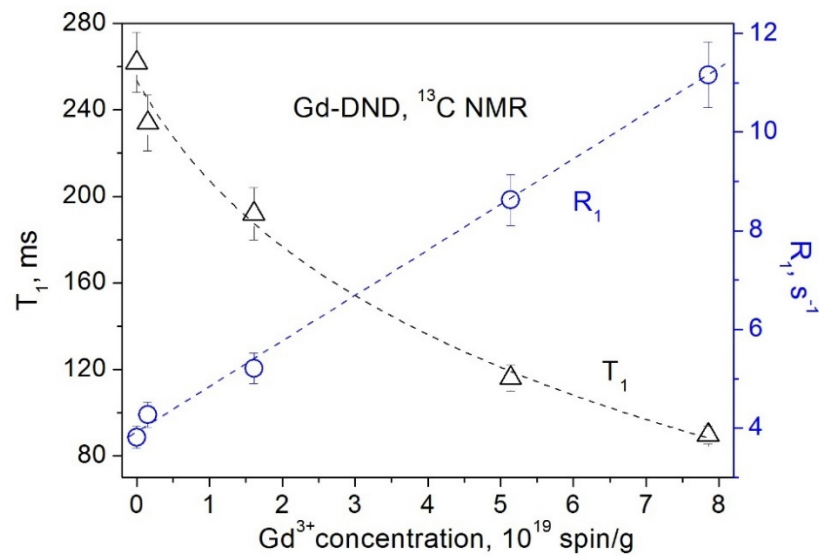


**Figure 7.** Dependence of the <sup>13</sup>C spin–lattice relaxation rate  $R_1$  (circles) and the spin–lattice relaxation time  $T_1$  (triangles) in Gd-DND powders on the  $Gd^{3+}$  ion concentration.

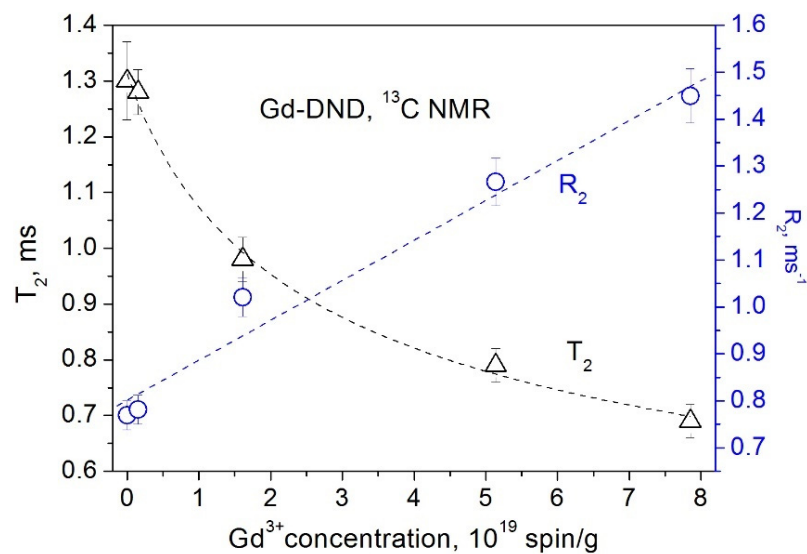


**Figure 8.** Dependence of the <sup>13</sup>C spin–spin relaxation rate  $R_2$  (circles) and the spin–spin relaxation time  $T_2$  (triangles) in Gd-DND powders on the  $Gd^{3+}$  ion concentration.

### 3.3. Powder HPHT Nanodiamonds

Let us move on to the powder nanodiamonds of the Syndia SYP series manufactured by L.M. Van Moppes & Sons SA (Switzerland) by milling the initial high-pressure high-temperature (HPHT) microdiamond crystallites with an average particle size of  $\sim 100 \mu\text{m}$ . According to the size distribution datasheets provided by the manufacturer, this milling process provides several SYP fractions with average particle sizes of 18, 30, 86, 132, 208, and 386 nm, respectively, which were used in our study along with the initial SYP micro CDFS of the size of  $100 \mu\text{m}$ . In Figure 9, we present our NMR measurements of SYP nanodiamonds of various sizes, in which the main contribution to relaxation is made by paramagnetic defects (mainly unpaired electron spins of broken bonds) associated with surface and subsurface defects that appear during the process of diamond

milling [27]. Such paramagnetic centers produced by mechanical damage (e.g., milling) are often found in insulators and semiconductors, including diamonds, and are observed in EPR experiments [38–41]. On diminishing the average size of the ND fraction, the density of these defects increases from  $7.6 \times 10^{18}$  spin/g in the fraction of the largest particle size to  $3.3 \times 10^{19}$  spin/g in the fraction of the smallest particle size. Figure 9 clearly shows the linear dependence of the spin–lattice relaxation rate and the hyperbolic dependence of the spin–lattice relaxation time on the concentration of the paramagnetic defects in this series of materials.

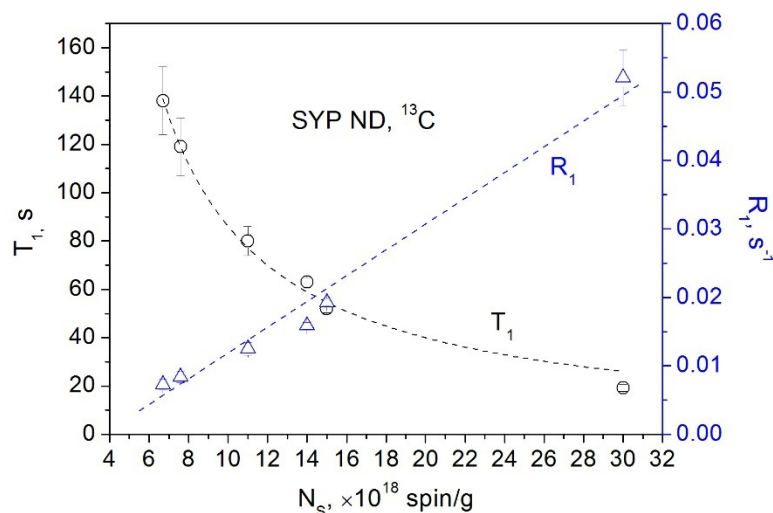


**Figure 9.** Dependence of the  $^{13}\text{C}$  spin–lattice relaxation rate  $R_1$  (triangles) and the spin–lattice relaxation time  $T_1$  (circles) in SYP nanodiamond powders on the concentration of the paramagnetic defects.

Hyperbolic-like concentration dependence of  $T_1$  was recently obtained in measurements of the  $^1\text{H}$  spin–lattice relaxation of aqueous solutions of nanodiamonds of 18 and 125 nm in diameter prepared by the HPHT technique [42].

The data obtained in our measurements demonstrate the universality of the dependence of the nuclear spin relaxation in nanodiamonds on the concentration of the paramagnetic centers both in suspensions and in powder samples. This is a universal law that is valid for solutions, suspensions, gels, and solids [12–16–18,22,23,27,29–31].

### 3.4. Other Materials Containing Gadolinium Ions

The universality of the dependences of nuclear spin relaxation in nanodiamonds on the concentration of paramagnetic centers in both suspensions and powder samples obtained in our measurements is supported by data on other non-diamond lanthanide complexes promising for NMR/MRI diagnostic probes [43]. For example, proton relaxation rates for  $\text{Gd}_2\text{O}_3$  nanodisks of different diameters and Gd-doped iron oxide nanoparticles of various sizes and shapes were measured in water after the nanoparticle surface functionalization with polyethylene glycol (PEG) dibasic acid. Both relaxation rates  $R_1$  and  $R_2$  reveal a linear dependence as a function of the Gd and Gd-Fe concentrations [44,45].

The relaxation rates  $R_1$  and  $R_2$  of water protons taken at room temperature in aqueous solutions of  $\text{SiO}_2$ -coated quantum dots with grafted Gd-DOTA complexes at various concentrations ranging from 0.125 to 4  $\mu\text{M}$  reveal a linear dependence on the Gd concentration [46].

Longitudinal relaxation rates and transverse relaxation rates as a function of concentration for aqueous solutions of gadolinium diethylenetriamine-pentaacetic acid

(Gd-DTPA) and gadolinium DTPA-bis methylamide (Gd-DTPA BMA) at 23 °C represent a linear regression of the data, from which the relaxation rates  $R_1$  and  $R_2$  were determined [47].

The  $R_1$  values of Gadomer (Gadolinium-1,4,7,10-tetraazacyclododecane- $N,N',N'',N'''$ -tetraacetic-monoamide-24-cascade-polymer), RESOVIST, or Ferucarbotran (a mixture of  $\text{Fe}_2\text{O}_3$  and  $\gamma\text{-Fe}_3\text{O}_4$  nanoparticles with a size of ~5 nm in a carboxydextran matrix), and GADOVIST ( $\text{C}_{18}\text{H}_{31}\text{GdN}_4\text{O}_9$ ) in bovine plasma, measured in a magnetic field of 1.5 T at 37 °C, show a linear dependence on the Gd concentration [48].

These results support well the above findings about the universality of the dependence of nuclear spin relaxation on the concentration of the paramagnetic centers both in suspensions and powder materials.

#### 4. Conclusions

It has been established that the dependences of the nuclear spin–lattice and spin–spin relaxation times and rates in nano- and microdiamonds on the concentration of intrinsic paramagnetic defects, surface-grafted ions, and milling-induced paramagnetic defects reveal a universal behavior for both suspensions and powder samples. The relaxation rates show linear concentration dependence, while the relaxation times exhibit hyperbolic dependence on the concentration of paramagnetic centers. This is a universal law that is valid for solutions, suspensions, gels, and solids. The data obtained will expand the understanding of the behavior of nanodiamonds and will be useful for their applications in quantum computing, spintronics, nanophotonics, and biomedicine. In our opinion, this is particularly important for the use of the nanodiamond suspensions as contrast agents and phantoms for MRI [16–18,20,49].

**Funding:** This research received no external funding.

**Acknowledgments:** I thank A.E. Aleksenskii, A.Ya. Vul', E.B. Yudina, and J.-P. Boudou for providing samples of micro- and nanodiamonds.

**Conflicts of Interest:** The authors declare no conflict of interest.

#### References

- Shenderova, O.A.; McGuire, G.E. Science and engineering of nanodiamond particle surfaces for biological applications (Review). *Biointerphases* **2015**, *10*, 030802.
- Arnault, J.C. Surface Modifications of Nanodiamonds and Current Issues for Their Biomedical Applications. In *Novel Aspects of Diamond, Topics of Applied Physics 121*; Yang, N., Ed.; Springer: Cham, Switzerland, 2015; Chapter 8, pp. 85–122.
- Komatsu, N. Chemical Functionalization of Nanodiamond for Nanobiomedicine. In *Synthesis and Applications of Nanocarbons*; Arnault, J.C., Eder, D., Eds.; Wiley: Hoboken, NJ, USA, 2020; Chapter 7, pp. 229–245.
- Nunn, N.; d'Amora, M.; Prabhakar, N.; Panich, A.M.; Froumin, N.; Torelli, M.D.; Vlasov, I.; Reineck, P.; Gibson, B.; Rosenholm, J.M.; et al. Fluorescent Single-Digit Detonation Nanodiamond for Biomedical Applications. *Methods Appl. Fluoresc.* **2018**, *6*, 035010.
- Wrachtrup, J.; Jelezko, F. Processing Quantum Information in Diamond. *J. Phys. Condens. Matter* **2006**, *18*, S807–S824.
- Doherty, M.W.; Manson, N.B.; Delaney, P.; Jelezko, F.; Wrachtrape, J.; Hollenberg, L.C.L. The Nitrogen-Vacancy Color Centre in Diamond. *Phys. Rep.* **2013**, *528*, 1–45.
- Shenderova, O.A.; Shames, A.I.; Nunn, N.A.; Torelli, M.D.; Vlasov, I.; Zaitsev, A. Review Article: Synthesis, Properties, and Applications of Fluorescent Diamond Particles. *J. Vac. Sci. Technol. B* **2019**, *37*, 030802.
- Aharonovich, I.; Neu, E. Diamond Nanophotonics. *Adv. Optical Mater.* **2014**, *2*, 911–928.
- Lv, X.; Walton, J.H.; Druga, E.; Wang, F.; Aguilar, A.; McKnelly, T.; Nazaryan, R.; Liu, F.L.; Wu, L.; Shenderova, O.; et al. Background-Free Dual-Mode Optical and  $^{13}\text{C}$  Magnetic Resonance Imaging in Diamond Particles. *Proc. Natl. Acad. Sci. USA* **2021**, *118*, e2023579118.
- Torelli, M.D.; Nunn, N.A.; Jones, Z.R.; Vedelaar, T.; Padamati, S.K.; Schirhagl, R.; Hamers, R.J.; Shames, A.I.; Danilov, E.O.; Zaitsev, A.; et al. High Temperature Treatment of Diamond Particles Toward Enhancement of Their Quantum Properties. *Front. Phys.* **2019**, *8*, 205.
- Pezzagna, S.; Meijer, J. Quantum Computer Based on Color Centers in Diamond. *Appl. Phys. Rev.* **2021**, *8*, 011308.
- Panich, A.M.; Shames, A.I.; Medvedev, O.; Osipov, V.Y.; Alexenskii, A.E.; Vul', A.Y. Magnetic Resonance Study of Detonation Nanodiamonds with Surface Chemically Modified by Transition Metal Ions. *Appl. Magn. Reson.* **2009**, *36*, 317–329.

13. Shames, A.I.; Panich, A.M.; Osipov, V.Y.; Aleksenskiy, A.E.; Vul', A.Y.; Enoki, T.; Takai, K. Structure and Magnetic Properties of Detonation Nanodiamond Chemically Modified by Copper. *J. Appl. Phys.* **2010**, *107*, 014318.
14. Panich, A.M.; Altman, A.; Shames, A.I.; Osipov, V.Y.; Alexenskiy, A.E.; Vul', A.Y. Proton Magnetic Resonance Study of Diamond Nanoparticles Decorated by Transition Metal Ions. *J. Phys. D Appl. Phys.* **2011**, *44*, 125303.
15. Panich, A.M.; Shames, A.I.; Sergeev, N.A.; Osipov, V.Y.; Alexenskiy, A.E.; Vul', A.Y. Magnetic Resonance Study of Gadolinium-Grafted Nanodiamonds. *J. Phys. Chem. C* **2016**, *120*, 19804–19811.
16. Panich, A.M.; Salti, M.; Goren, S.D.; Yudina, E.B.; Alexenskii, A.E.; Vul', A.Y.; Shames, A.I. Gd(III)-Grafted Detonation Nanodiamonds for MRI Contrast Enhancement. *J. Phys. Chem. C* **2019**, *123*, 2627–2631.
17. Panich, A.M.; Shames, A.I.; Goren, S.D.; Yudina, E.B.; Aleksenskii, A.E.; Vul', A.Y. Examining relaxivities in suspensions of nanodiamonds grafted by magnetic entities—Comparison of two approaches. *Magn. Reson. Mater. Phys. Biol. Med.* **2020**, *33*, 885–888.
18. Panich, A.M.; Salti, M.; Prager, O.; Swissa, E.; Kulvelis, Y.V.; Yudina, E.B.; Aleksenskii, A.E.; Goren, S.D.; Vul', A.Y.; Shames, A.I. PVP-coated Gd-grafted nanodiamonds as a novel and potentially safer contrast agent for in-vivo MRI. *Magn. Reson. Med.* **2021**, *86*, 935–942.
19. Panich, A.M.; Aleksenskii, A.E.; Yudina, E.B.; Vul', A.Y. Spatially Resolved Spin–Lattice Relaxation Times and Line Widths in Manganese-Grafted Detonation Nanodiamonds. *J. Phys. Chem. C* **2022**, *126*, 1489–1495.
20. Panich, A.M.; Shames, A.I.; Aleksenskii, A.E.; Yudina, E.B.; Vul', A.Y. Manganese-grafted detonation nanodiamond, a novel potential MRI contrast agent. *Diamond Relat. Mater.* **2021**, *119*, 108590.
21. Sękowska, A.; Majchrowicz, D.; Sabisz, A.; Ficek, M.; Bułko-Piontecka, B.; Kosowska, M.; Jing, L.; Bogdanowicz, R.; Szczerska, M. Nanodiamond phantoms mimicking human liver: Perspective to calibration of T<sub>1</sub> relaxation time in magnetic resonance imaging. *Sci. Rep.* **2020**, *10*, 6446–6452.
22. Abragam, A. *The Principles of Nuclear Magnetism*; Clarendon Press: Oxford, UK, 1961.
23. Bloembergen, N. Proton Relaxation Times in Paramagnetic Solutions. *J. Chem. Phys.* **1957**, *27*, 572–573.
24. Solomon, I. Relaxation processes in a system of two spins. *Phys. Rev.* **1955**, *99*, 559–565.
25. Aleksenskiy, A.E.; Eydelman, E.; Vul', A.Y. Deagglomeration of Detonation Nanodiamonds. *Nanosci. Nanotechnol. Lett.* **2011**, *3*, 68–74.
26. Shames, A.I.; Panich, A.M.; Kempinski, W.; Alexenskii, A.E.; Baidakova, M.V.; Dideikin, A.T.; Osipov, V.Y.; Siklitski, V.I.; Osawa, E.; Ozawa, M.; et al. Defects and impurities in nanodiamonds: EPR, NMR and TEM study. *J. Phys. Chem. Solids* **2002**, *63*, 1993–2001.
27. Panich, A.M.; Sergeev, N.A.; Shames, A.I.; Osipov, V.Y.; Boudou, J.P.; Goren, S.D. Size dependence of <sup>13</sup>C nuclear spin-lattice relaxation in micro- and nanodiamonds. *J. Phys. Condens. Matter* **2015**, *27*, 072203.
28. Shames, A.I.; Panich, A.M.; Porro, S.; Rovere, M.; Musso, S.; Tagliaferro, A.; Baidakova, M.V.; Osipov, V.Y.; Vul', A.Y.; Enoki, T.; et al. Defects localization and nature in bulk and thin film ultrananocrystalline diamond. *Diamond Relat. Mater.* **2007**, *16*, 1806–1812.
29. Shames, A.I.; Panich, A.M. Paramagnetic Defects in Nanodiamonds. In *Nanodiamonds: Advanced Material Analysis, Properties and Applications*; Arnault, J.C., Ed.; Elsevier: Amsterdam, The Netherlands, 2017; Chapter 6, pp. 131–154.
30. Panich, A.M. Nuclear Magnetic Resonance Studies of Nanodiamonds. *Crit. Rev. Solid State Mater. Sci.* **2012**, *37*, 276–303.
31. Panich, A.M. Nuclear Magnetic Resonance Studies of Nanodiamond Surface Modification. *Diamond Relat. Mater.* **2017**, *79*, 21–31.
32. Osipov, V.; Shames, A.; Enoki, T.; Takai, K.; Baidakova, M.; Vul', A. Paramagnetic defects and exchange coupled spins in pristine ultrananocrystalline diamonds. *Diamond Relat. Mater.* **2007**, *16*, 2035–2038.
33. Enoki, T.; Kobayashi, Y.; Katsuyama, C.; Osipov, V.; Baidakova, M.; Takai, K.; Fukui, K.; Vul', A. Structures and electronic properties of surface/edges of nanodiamond and nanographite. *Diam. Relat. Mater.* **2007**, *16*, 2029–2034.
34. Fukushima, E.; Roeder, S.B.W. *Experimental Pulse NMR. A Nuts and Bolts Approach*; Addison-Wesley: London, UK, 1981; p. 539.
35. Panich, A.M.; Furman, G.B. Nuclear spin-lattice relaxation and paramagnetic defects in carbon nanomaterials. *Diam. Relat. Mater.* **2012**, *23*, 157–161.
36. Meiboom, S.; Gill, D. Modified Spin-Echo Method for Measuring Nuclear Relaxation Times. *Rev. Sci. Instrum.* **1958**, *29*, 688–691.
37. Zhao, L.; Shiino, A.; Qin, H.; Kimura, T.; Komatsu, N. Synthesis, Characterization, and Magnetic Resonance Evaluation of Polyglycerol-Functionalized Detonation Nanodiamond Conjugated with Gadolinium(III) Complex. *J. Nanosci. Nanotechnol.* **2015**, *15*, 1076–1082.
38. Samsonenko, N.D.; Sobolev, E.V. Electron Paramagnetic Resonance Produced by Surface of Diamond. *Pis'ma Zh. Eksp. Teor. Fiz.* **1967**, *5*, 304–307.
39. Samsonenko, N.D.; Zhmykhov, G.V.; Zon, V.H.; Aksenov, V.K. Characteristic Features of the Electron Paramagnetic Resonance of the Surface Centers of Diamond. *J. Struct. Chem.* **1979**, *20*, 951–953.
40. Walters, G.K.; Estle, T.L. Paramagnetic Resonance of Defects Introduced Near the Surface of Solids by Mechanical Damage. *J. Appl. Phys.* **1961**, *32*, 1854–1859.
41. Higinbotham, J.; Haneman, D. Electron paramagnetic resonance from germanium surfaces. *Surf. Sci.* **1970**, *19*, 39–44.
42. Waddington, D.E.J. *Diamonds on the Inside: Imaging Nanodiamonds with Hyperpolarized MRI*. Ph.D. Thesis, The University of Sydney, Sydney, Australia, 2018.

43. Zapolotsky, E.N.; Qu, Y.; Babailov, S.P. Lanthanide complexes with polyaminopolycarboxylates as prospective NMR/MRI diagnostic probes: Peculiarities of molecular structure, dynamics and paramagnetic properties. *J. Incl. Phenom. Macrocycl. Chem.* **2022**, *102*, 1–33.
44. Singh, G.; McDonagh, B.H.; Hak, S.; Peddis, D.; Bandopadhyay, S.; Sandvig, I.; Sandvig, A.; Glomm, W.R. Synthesis of gadolinium oxide nanodisks and gadolinium doped iron oxide nanoparticles for MR contrast agents. *J. Mater. Chem. B* **2017**, *5*, 418–422.
45. Caspani, S.; Magalhaes, R.; Araujo, J.P.; Sousa, C.T. Magnetic nanomaterials as contrast agents for MRI. *Materials* **2020**, *13*, 2586.
46. Gerion, D.; Herberg, J.; Bok, R.; Gjersing, E.; Ramon, E.; Maxwell, R.; Kurhanewicz, J.; Budinger, T.F.; Gray, J.W.; Shuman, M.A.; et al. Paramagnetic Silica-Coated Nanocrystals as an Advanced MRI Contrast Agent Daniele. *J. Phys. Chem. C* **2007**, *111*, 12542–12551.
47. Reichenbach, J.R.; Hacklander, T.; Harth, T.; Hofer, M.; Rassek, M.; Modder, U.  $^1\text{H}$   $T_1$  and  $T_2$  measurements of the MR imaging contrast agents Gd-DTPA and Gd-DTPA BMA at 1.5T. *Eur. Radiol.* **1997**, *7*, 264–274.
48. Rohrer, M.; Bauer, H.; Mintorovitch, J.; Requardt, M.; Weinmann, H.J. Comparison of Magnetic Properties of MRI Contrast Media Solutions at Different Magnetic Field Strengths. *Investig. Radiol.* **2005**, *40*, 715–724.
49. Panich, A.M. Can detonation nanodiamonds serve as MRI phantoms? *Magn. Reson. Mater. Phys. Biol. Med.* **2022**, *35*, 345–347.